RESEARCH ARTICLE | OCTOBER 21 2025

Enhanced UV detection in GaN-based photodetectors through InN/AlN heterostructure integration and doping-engineered PIN architecture

M. Kilin ; O. Tanriverdi; B. Karahan ; F. Yasar

AIP Advances 15, 105126 (2025)
https://doi.org/10.1063/5.0295485

Enhanced UV detection in GaN-based photodetectors through InN/AlN heterostructure integration and doping-engineered PIN architecture

Cite as: AIP Advances 15, 105126 (2025); doi: 10.1063/5.0295485
Submitted: 8 August 2025 • Accepted: 5 October 2025 •
Published Online: 21 October 2025

M. Kilin,[1,a] O. Tanriverdi,[2] B. Karahan,[3] and F. Yasar[4]

AFFILIATIONS

[1] Medical Science and Optics Department, Adiyaman University, Adiyaman, Turkey
[2] Electrical and Electronics Engineering Department, Adiyaman University, Adiyaman, Turkey
[3] Electrical and Electronics Engineering Department, Hasan Kalyoncu University, Gaziantep, Turkey
[4] Microdevices Laboratory, Jet Propulsion Laboratory, NASA, Pasadena, California 91109, USA

[a] **Author to whom correspondence should be addressed:** mkilin@adiyaman.edu.tr

ABSTRACT

This study presents a comprehensive simulation-based optimization of gallium nitride (GaN)-based metal–semiconductor–metal (MSM) photodetectors designed for ultraviolet (UV) applications. The proposed device architecture incorporates a novel indium nitride/gallium nitride/aluminum nitride (InN/GaN/AlN) heterostructure integrated on a sapphire substrate, combined with refined doping strategies and interdigitated electrode geometry. By systematically analyzing the effects of mesa layer thickness, buffer layers, substrate type, and doping concentrations, we demonstrate significant enhancements in photocurrent generation, photoabsorption rate, and spectral responsivity. Notably, replacing the conventional sapphire substrate with silicon carbide (SiC) and introducing low-level p-type and n-type (p–n) doping into the GaN region enables p–i–n diode-like behavior, contributing to reduced dark current and improved UV selectivity. Building upon these structural enhancements, the final geometric optimization of the nickel/gold (Ni/Au) electrode fingers led to an approximately eightfold increase in photocurrent compared to the initial design, representing the most significant contribution to the improvement in absorption efficiency. These findings offer an effective route for designing next-generation MSM photodetectors with improved sensitivity, noise performance, and thermal compatibility, suitable for high-performance ultraviolet detection applications.

I. INTRODUCTION

GaN is a wide bandgap semiconductor material that has demonstrated remarkable potential for optoelectronic applications, particularly in the UV range.[1–5] Its direct bandgap of ~3.4 eV enables intrinsic UV sensitivity without the need for additional optical filtering.[6,7] In addition, GaN exhibits excellent thermal stability, high carrier mobility, and strong radiation hardness, making it suitable for high-performance UV photodetectors.[8–14] MSM photodetectors are popular because they are easy to fabricate, operate at high speeds, and are compatible with large-scale integration.[15–17] However, optimizing the design parameters of GaN MSM photodetectors is crucial for maximizing their performance. This includes fine-tuning the thickness of the GaN active layer,[18] optimizing the geometry of the metal fingers,[19,20] exploring alternative active layer structures,[21–23] doping the GaN thin film,[24,25] and selecting the most suitable substrate for device fabrication.[26–28] The thickness of the GaN active layer significantly influences light absorption, carrier transport, and device efficiency. A thicker GaN layer absorbs more light and improves responsivity but slows down the response.[29] A very thin GaN layer, on the other hand, does not absorb enough UV light, reducing the photocurrent.[30] Therefore, an optimized

GaN thickness is essential for balancing responsivity and speed. The metal electrode design, including finger width, spacing, and aspect ratio, incorporates these components. A reduced finger spacing enhances the electric field, improving carrier drift velocity and response speed, but may also increase dark current due to tunneling effects.[31] In addition, the choice of Schottky contact metals affects the barrier height, influencing the noise performance of the device.[32]

The optimization of the geometric design of metal fingers is critical to achieving an optimal balance between high-speed operation and low-noise performance.[33] To enhance the optoelectronic performance of UV photodetectors beyond geometrical optimization, AlN/GaN/InN multilayer heterostructures have been strategically engineered to exploit their complementary bandgaps and polarization-induced electric fields, enabling efficient carrier generation and transport.[34] The wide bandgap and strong spontaneous polarization of AlN (6.2 eV) serve to confine carriers and suppress leakage currents, while the intermediate GaN layer (3.4 eV) functions as the primary absorption region.[35] Finally, an ultrathin InN interlayer (0.7 eV) introduces strong interfacial electric fields and energy band bending, significantly enhancing carrier separation and responsivity in the deep-UV regime.[36] Similarly, GaN nanowires and quantum dots increase the active surface area, enhancing light absorption and carrier collection efficiency.[37] The choice of substrate affects the material quality, strain effects, and overall device performance. Commonly used substrates for GaN growth include sapphire and SiC.[38,39] Sapphire is cost-effective and optically transparent in the UV range but suffers from a high lattice mismatch with GaN, leading to dislocations.[40] SiC, on the other hand, provides better lattice matching and superior thermal conductivity, making it a preferred choice for high-power and high-temperature applications.[41] The optimization of GaN MSM photodetectors involves a multifaceted approach, including material selection, structural design, and substrate engineering. By carefully tuning these parameters, significant improvements in responsivity, speed, and noise characteristics can be achieved. This study presents a systematic optimization strategy aimed at enhancing the performance of GaN MSM photodetectors, contributing to the advancement of high-efficiency UV photodetection technologies.

II. MATERIAL AND DESIGN

The performance of MSM photodetectors strongly depends on the coordinated selection of materials and structural design parameters.[42] Table I summarizes key physical properties such as lattice parameters, bandgap energies, and thermal conductivities of the semiconductors and metals used in this study. These parameters collectively affect the electrical field distribution, optical absorption, and thermal stability of the device.

GaN is employed as the main active layer due to its direct bandgap, which provides strong UV absorption with relatively high electron mobility.[45] To improve lattice compatibility and reduce defect-related recombination, AlN is used as a buffer layer, while InN is integrated as an ultra-thin (about $x < 0.005$ μm) interlayer to enhance carrier confinement.[46] These III-nitride combinations also allow partial band engineering, which contributes to more efficient carrier separation without significantly increasing complexity.

The choice of substrate, either sapphire or SiC, directly influences both lattice matching and thermal performance.[47] While sapphire offers transparency and cost-effectiveness, SiC provides superior thermal conductivity and mechanical robustness, making it favorable for high-power or elevated-temperature applications.

Doping concentration is another critical factor that modulates carrier dynamics in MSM photodetectors. Within the proposed AlN/GaN/InN heterostructure, the AlN layer, typically insulating, can be engineered with light *p*-type GaN doping to enhance hole transport and serve as an effective buffer for carrier separation. Conversely, the InN region can benefit from *n*-type GaN doping, optimizing electron mobility while mitigating recombination losses. This selective doping strategy not only facilitates efficient charge separation but also refines the internal electric field profile. Stepwise optimization of doping concentrations, ranging from 1×10^{1} to 1×10^{19} cm^{-3}, has been shown to significantly influence both charge transport characteristics and the spatial distribution of the electric field.[48]

Finally, the geometry and material of the metal electrodes play a decisive role in determining device responsivity and speed. Interdigitated finger structures are optimized in width, spacing,

TABLE I. Key material properties of semiconductors and metals used in photodetectors.

Material[a]	Lattice parameters	Bandgap (eV)	Thermal conductivity (W/m·K)
Sapphire (Al_2O_3)	a = 4.76, c = 12.99	Transparent in UV	35
SiC (4H SiC)	a = 3.08, c = 15.12	3.2	120–180
GaN	a = 3.189, c = 5.185	3.4	130
InN	a = 3.54, c = 5.70	0.7	45
AlN	a = 3.11, c = 4.98	6.2	285
Ni	a = 3.52	Metal	90
Au	a = 4.08	Metal	317

[a]Material parameters such as bandgap and thermal conductivity are taken from experimental and theoretical studies.[7,26,43,44] These values serve as reference inputs for photodetector simulations.

and thickness to control electric field intensity and carrier transit times.[19,20] To achieve suitable Schottky barrier heights and stable contact behavior, Ni/Au is selected as the electrode pair due to its well-established work function alignment with GaN.[49]

The schematic representation of the proposed MSM photodetector structure is detailed in Fig. 1. As illustrated in Fig. 1(a), the device operates based on a back-to-back Schottky contact configuration, which leads to charge accumulation at the metal–semiconductor interfaces. The corresponding design of the interdigitated metal fingers, including the dimensions and arrangement of the floating Au and Ni layers, is presented in Fig. 1(b). Furthermore, Fig. 1(c) compares the final device architectures fabricated on sapphire and SiC substrates, both incorporating a mesa structure formed by AlN, GaN, and an ultrathin InN interlayer. These visualizations collectively support the material and structural choices discussed in this section.

This integrated material and design approach aims not to fully eliminate all limitations but to address key performance bottlenecks with coordinated structural improvements across the device architecture.

III. SIMULATIONS AND METHODOLOGY

The simulation process was conducted using the Silvaco Atlas TCAD environment to investigate and optimize the performance of GaN-based MSM UV photodetectors. All models were constructed in two dimensions under steady-state conditions at room temperature (300 K), solving the Poisson equation and carrier continuity equations self-consistently. The physical models included drift-diffusion transport, thermionic emission at Schottky contacts, and field-dependent mobility effects. Each simulation step focused on enhancing one or more performance metrics such as photocurrent, photoabsorption rate, or spectral responsivity.

Initially, a baseline structure consisting of a sapphire substrate, GaN active region, and Ni/Au electrodes was modeled to evaluate the impact of GaN mesa thickness. The GaN layer thickness was varied from 0.1 to 1.0 μm, and the optimal absorption rate was obtained at h_{GaN} = 0.4 μm, where the trade-off between light penetration depth and carrier transport was best balanced.

Subsequently, an AlN buffer layer and an almost ultrathin InN surface layer were integrated into the mesa to form a novel AlN/GaN/InN heterostructure. While the AlN thickness was fixed

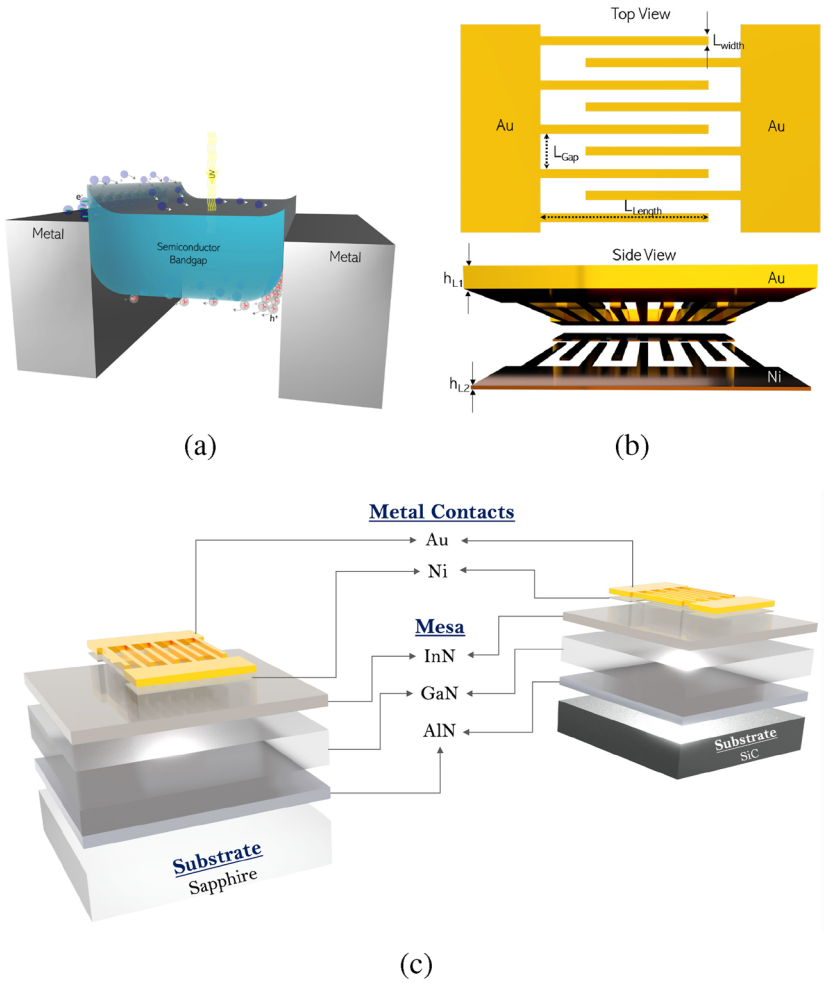

FIG. 1. Visual representation of the MSM photodetector: (a) Band diagram showing back-to-back Schottky barriers. (b) Metal finger structure of Au/Ni thin films. (c) Fabricated device layout on sapphire and SiC substrates.

at h_{AlN} = 0.1 μm, the InN layer thickness was varied from 0.01 to 0.1 μm, with maximum photoabsorption observed at h_{InN} = 0.01 μm. This configuration exploited the polarization-induced electric field at the heterointerfaces, leading to improved carrier separation and internal electric field modulation. The AlN layer served as a strain-relieving buffer between sapphire and GaN, improving crystalline quality without completely eliminating mismatch-related defects.

To evaluate the substrate effect, sapphire was replaced by SiC in an identical layer configuration. The SiC-based design demonstrated enhanced thermal conductivity and photocurrent under identical bias conditions, offering better high-temperature stability and increased UV response.

Following the heterostructure optimization, doping profiles were introduced into the GaN region to induce p–i–n diode-like behavior in the MSM configuration. A three-layer GaN stack was created with symmetric p-type and n-type doping around an undoped GaN core. Doping concentrations were swept from 1×10^{1} to 1×10^{19} cm^{-3}, with optimal values of $doping_{p-type} = 1 \times 10^{5}$ cm^{-3} for p-type and $doping_{n-type} = 1 \times 10^{12}$ cm^{-3} for n-type layers. This configuration enhanced the internal electric field and reduced the dark current while maintaining high responsivity.

Finally, the interdigitated electrode geometry was refined to maximize the absorption and carrier collection efficiency. The Ni layer thickness was fixed at h_{Ni} = 0.01 μm, while the Au layer thickness was varied from 0.1 to 0.2 μm. The highest absorption was recorded at h_{Au} = 0.12 μm Au thickness. Finger widths and gaps were then co-optimized, with the best configuration determined as L_{Width} = 8.0 μm and L_{Gap} = 19 μm. All geometrical and material variations were evaluated based on their impact on current–voltage (I–V) characteristics, absorption profiles, and UV spectral responsivity.

Throughout the simulation, fine meshing was applied around the heterojunctions and metal-semiconductor interfaces to ensure numerical stability and accurate field distribution. The results were verified across multiple bias conditions to confirm robustness. While the simulations predict substantial performance improvements, potential discrepancies arising from interface defects or fabrication limitations are acknowledged and considered in the discussion.

To represent bulk defect recombination in an effective manner, Shockley–Read–Hall (SRH) statistics with literature-consistent electron and hole lifetimes were employed within the GaN region, while Schottky contacts were modeled via thermionic emission with field-dependent mobility. These choices capture first-order defect-limited recombination and contact-region field effects. We note that our comparative conclusions rely on relative trends across device variants, which remain robust under reasonable variations of SRH lifetimes. A detailed benchmarking of the baseline device against experimental responsivity and PDCR is provided in Sec. IV A (MSM-Ref).

To further ensure the reliability of the employed TCAD framework, the selected physical parameters, including bandgap energies, carrier mobilities, and Schottky barrier heights, were validated by comparison with experimentally reported GaN MSM photodetectors. A detailed benchmarking of responsivity and PDCR values is presented in Sec. IV A (MSM-Ref), where the calibration of the baseline device against established experimental results is explicitly discussed.

IV. RESULTS AND DISCUSSION

This section presents a comparative analysis of the simulated performance metrics obtained from a series of sequential structural optimizations applied to GaN-based MSM UV photodetectors. All design variants were modeled using Silvaco Atlas TCAD and evaluated based on their impact on key figures of merit, including photocurrent generation, photoabsorption rate, and spectral responsivity. For clarity and brevity throughout this section, each configuration is denoted with a specific abbreviation: MSM-Ref (baseline sapphire/GaN/Ni/Au structure with optimized mesa thickness), MSM-Buffer (sapphire/AlN/GaN/InN/Ni/Au incorporating AlN and InN buffer layers), MSM-SiC (SiC/AlN/GaN/InN/Ni/Au employing a SiC substrate), MSM-PIN (sapphire/p-GaN/GaN/n-GaN/Ni/Au introducing p–i–n-like doping), and MSM-Opt (final design with optimized Ni/Au electrode geometry). Rather than reporting results in isolation, the analysis focuses on relative comparisons between these configurations under consistent biasing conditions, thereby elucidating both the individual contributions and cumulative enhancements introduced at each design stage. This approach enables a comprehensive understanding of how systematic structural modifications influence the overall photodetector performance.

A. MSM-ref: Sapphire/GaN/Ni/Au

The initial simulation phase focused on the reference MSM photodetector structure composed of a GaN active layer (h_{GaN} = 0.4 μm) deposited on a sapphire substrate with Ni/Au interdigitated electrodes. As illustrated in Fig. 2(a), the I–V characteristics under UV illumination (360 nm) exhibit a pronounced asymmetry due to the back-to-back Schottky barrier configuration. The photocurrent reaches a peak value of ~2.74×10^{-8} A at +3 V, while the dark current remains significantly lower, around 5.73×10^{-14} A, outperforming the results reported in Ref. 50, resulting in a photo-to-dark current ratio (PDCR) exceeding 1.74×10^{7} [Fig. 2(b)], exhibiting a higher PDCR than that reported in Refs. 51 and 52. This high ratio indicates strong signal-to-noise characteristics and effective suppression of leakage pathways. The spectral responsivity, shown in Fig. 2(c), remains centered around 360 nm with an amplitude consistent with the intrinsic absorption edge of GaN. At this wavelength, a responsivity of 0.5275 A/W is achieved, validating the baseline structure and establishing a quantitative foundation for evaluating subsequent heterostructural and geometrical optimizations. This responsivity value notably surpasses that reported by Butun *et al.*, who achieved 0.23 A/W at 356 nm under similar bias conditions.[51] In addition, the photon absorption rate (par) in the GaN region reaches ~1.51×10^{24} par/cm^{3} s, as determined by the optical intensity distribution across the mesa geometry. This value reflects the strong confinement and penetration of incident UV radiation within the active layer, reinforcing the effectiveness of the vertical photogeneration profile in this baseline configuration.

Building upon the baseline performance, the MSM-Ref configuration establishes a reliable reference point for assessing further enhancements. While the results demonstrate excellent dark current suppression and UV responsivity, certain intrinsic limitations remain—particularly in terms of strain management, electric field

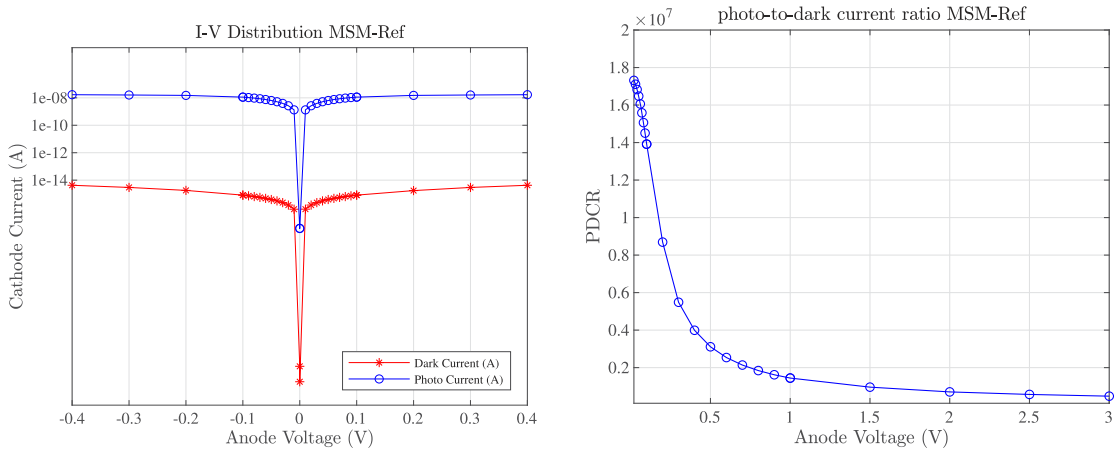

(a) (b)

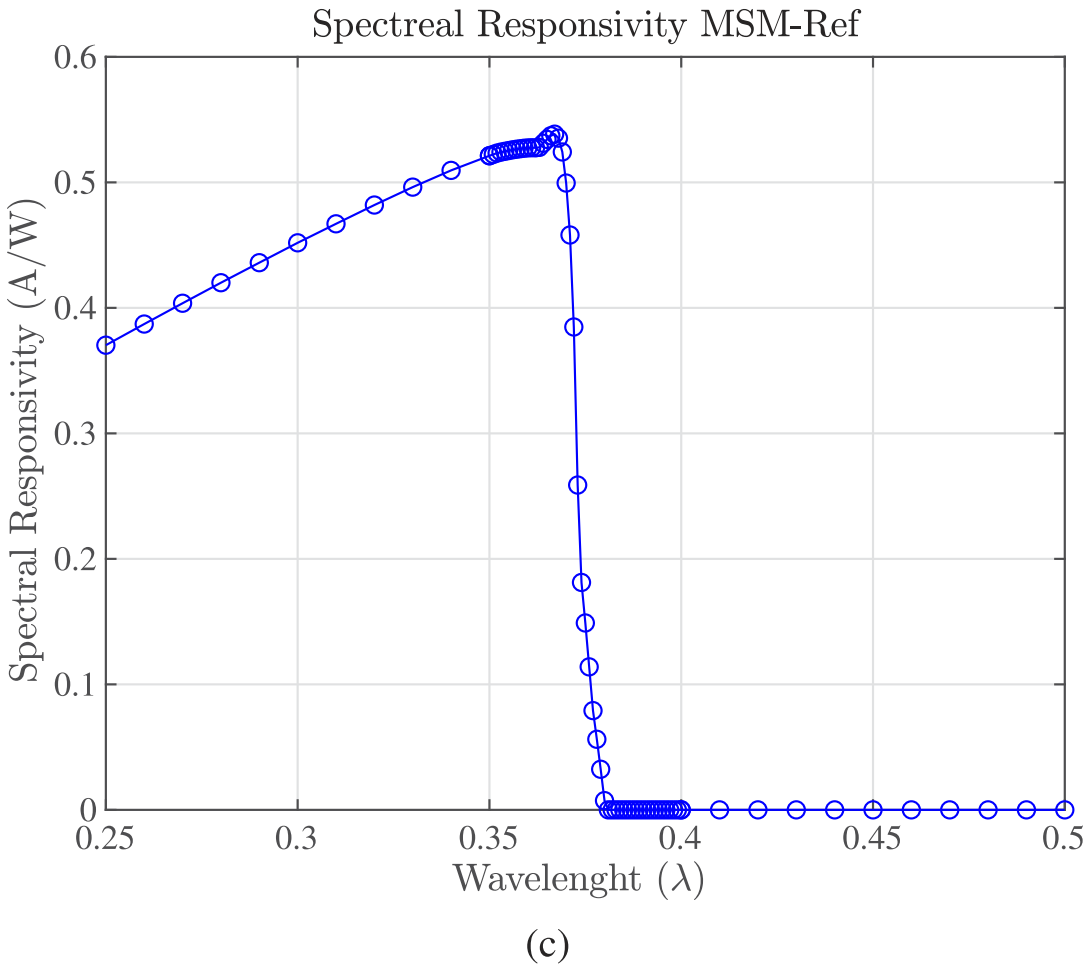

(c)

FIG. 2. MSM-Ref detector structure for the optimized GaN layer thickness of 0.4 μm: (a) I–V distribution, (b) PDCR, and (c) spectral responsivity A/W.

modulation, and carrier separation efficiency. To address these aspects, the following device iterations explore the inclusion of an AlN buffer to alleviate lattice mismatch, the use of an ultrathin InN interlayer to enhance internal electric fields, the substitution of sapphire with SiC for improved thermal and structural compatibility, and the introduction of p-type and n-type doping to induce p–i–n diode-like characteristics. Electrode geometry is also refined to optimize optical absorption and charge collection. These progressive modifications are examined in detail in Secs. IV B–IV D, each designed to build upon the foundation established by the reference device.

B. MSM-Buffer:Sapphire/AlN/GaN/InN/Ni/Au

1. MSM-SiC: SiC/AlN/GaN/InN/Ni/Au

In order to extend the MSM-Ref design, structural variations were introduced by incorporating a mesa region composed of an AlN/GaN/InN heterostructure, followed by replacing the sapphire substrate with SiC to assess substrate-induced effects. The design-related optimization processes were detailed in Sec. III. The first configuration, MSM-Buffer, yielded a peak photocurrent of 3.23×10^{-7} A and a dark current of 2.69×10^{-14} A, corresponding to a PDCR of 1.97×10^{7}, a photoabsorption rate of ~1.5×10^{24} par/cm^3 s, and a responsivity of 0.6224 A/W. Compared to the MSM-Ref, these results reflect an enhancement in responsivity and a further suppression of dark current, attributable to the InN interlayer's modulation of the internal electric field and the AlN buffer's role in lattice strain mitigation. In contrast, the second configuration, MSM-SiC, while benefiting from improved lattice matching and thermal conductivity, showed a lower peak photocurrent of 3.09×10^{-8} A and a higher dark current of 2.68×10^{-13} A. Consequently, the PDCR dropped to 3.5×10^{5}, and responsivity decreased to 0.4463 A/W, with the photoabsorption rate settling around 7×10^{22} par/cm^3 s. These performance shifts suggest that while SiC substrates enhance thermal robustness, the concurrent modifications to the electric field distribution and carrier dynamics may limit photocurrent gain in this heterostructure context. Nevertheless, both configurations demonstrate structurally tunable performance, forming a foundation upon which additional enhancements, such as doping-induced p–i–n diode-like profiles and electrode geometry optimization, can be systematically built.

In addition to the present TCAD simulations at 300 K, the superior thermal conductivity of SiC provides clear evidence for more stable performance at elevated temperatures. This expectation is not only supported by previous experimental studies of GaN-based photodetectors on SiC substrates but also confirmed by our recent thermal analysis, which demonstrated enhanced heat dissipation and improved operational stability in SiC-based architectures.[14] These results reinforce the reliability of the SiC substrate for high-temperature operation.

C. MSM-PIN: sapphire/p_{GaN}/GaN/n_{GaN}/Ni/Au

Since the anticipated photocurrent enhancement in the MSM-SiC structure engineered by replacing the sapphire substrate with SiC was found to be limited primarily to thermal effects, subsequent structural development focused on improving the MSM-Buffer configuration. To this end, a p–i–n diode-like architecture was introduced through strategic doping profile engineering, aiming to establish a built-in electric field and thereby enhance carrier separation and overall device responsivity. A symmetric doping profile was implemented on the MSM-Buffer heterostructure by introducing p-type and n-type GaN layers surrounding an intrinsic

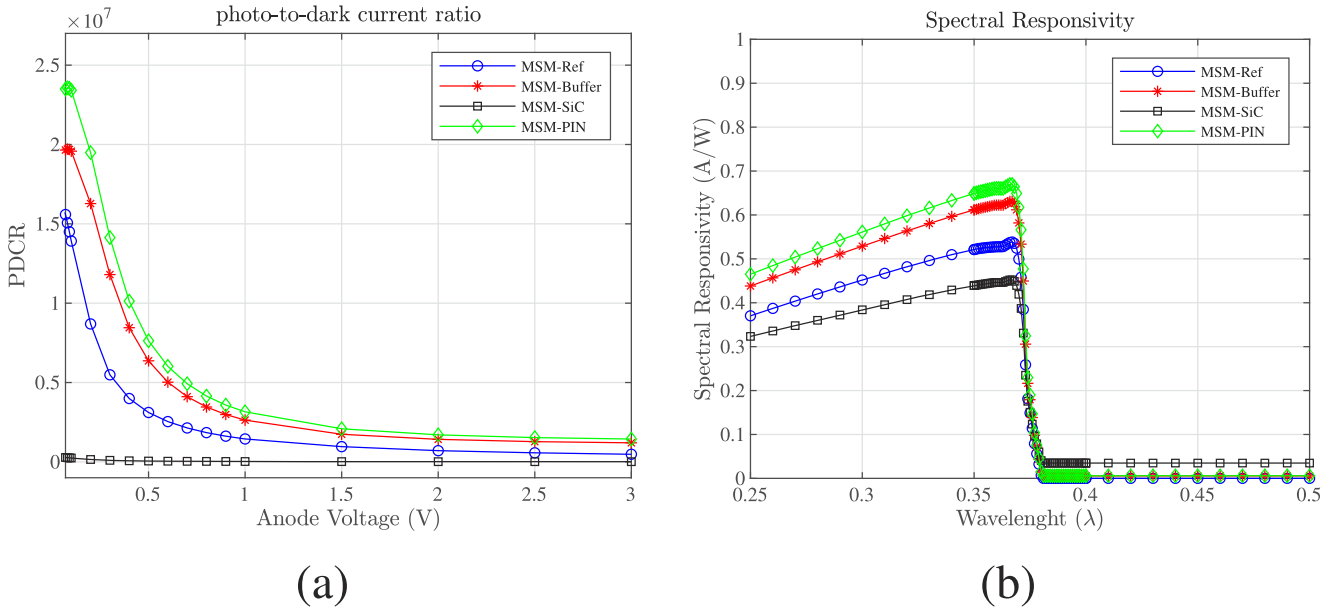

FIG. 3. Presents a comparative analysis of four MSM designs: (a) PDCR and (b) spectral responsivity.

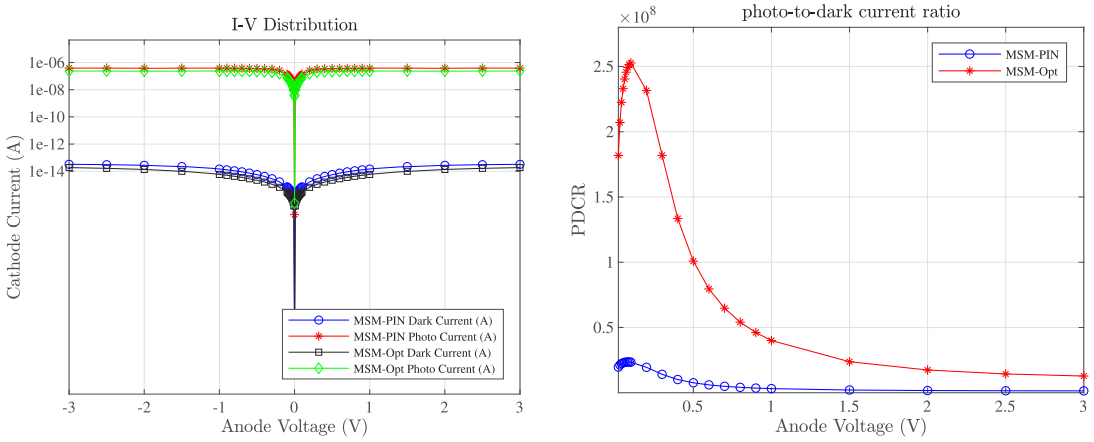

(a) (b)

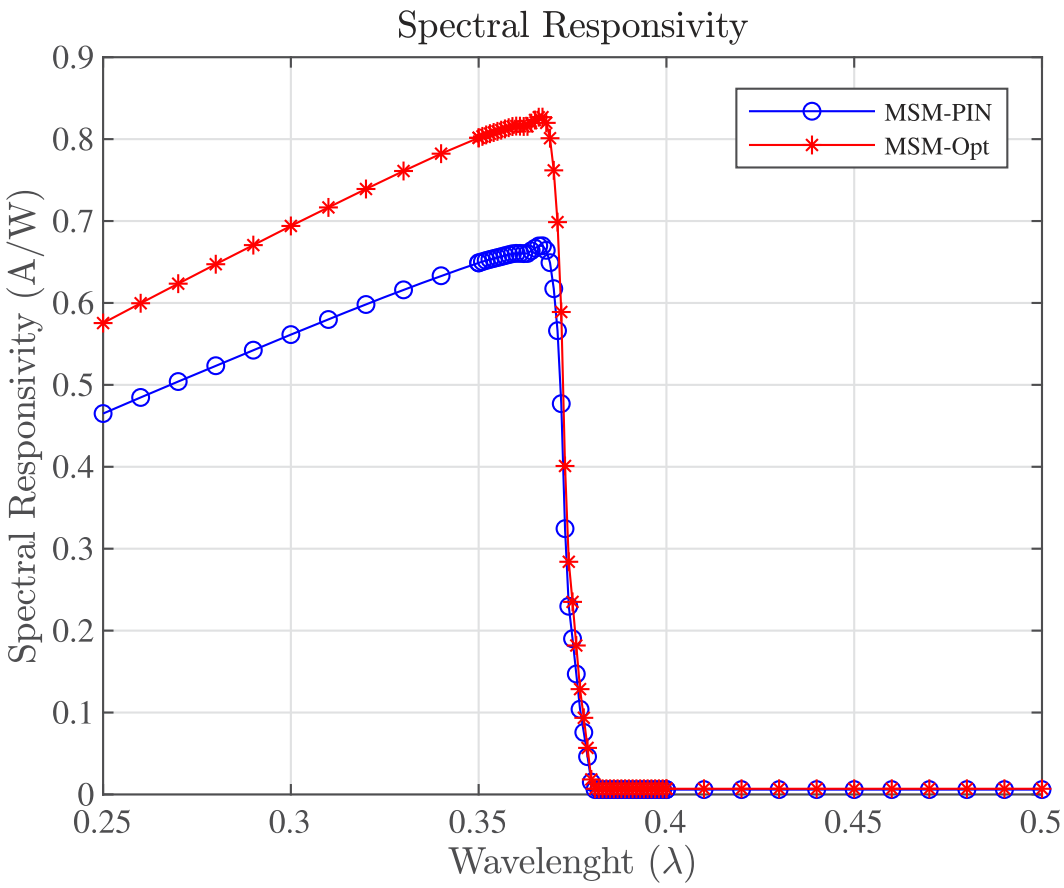

(c)

FIG. 4. Comparison of the two best-performing MSM photodetector configurations: the sapphire/p-GaN/GaN/n-GaN/Ni/Au structure and the geometry-optimized sapphire/AlN/GaN/InN/Ni/Au structure. (a) Current–voltage (I–V) characteristics under UV illumination (360 nm), highlighting enhanced carrier transport in the geometry-optimized device at higher bias. (b) PDCR across both structures, showing superior signal-to-noise performance in the geometry-optimized configuration. (c) Spectral responsivity comparison, indicating improved responsivity and sharper UV selectivity for the electrode-optimized design.

GaN core, as described in Sec. III. This modified device configuration, MSM-PIN: sapphire/p-GaN/GaN/n-GaN/Ni/Au, produced a photocurrent of 3.88×10^{-7} A and a dark current of 3.24×10^{-14} A, resulting in a PDCR of 2.35×10^{7} and a photoabsorption rate of ~2.2×10^{24} par/cm^3 s. A responsivity of 0.6605 A/W was achieved, surpassing all previously examined structures in both magnitude and spectral sharpness. These improvements can be attributed to the built-in electric field across the p–i–n profile, which enhances carrier separation efficiency and reduces recombination losses. As illustrated in Fig. 3(a), the PDCR of the doped structure closely approaches that of the best-performing undoped design, while offering improved stability under bias. In addition, the spectral responsivity curve shown in Fig. 3(b) confirms a sharper UV selectivity with minimal response leakage into longer wavelengths. Considering all four configurations examined, namely MSM-Ref, MSM-Buffer, MSM-SiC, and MSM-PIN, demonstrates the most balanced trade-off between signal strength, noise suppression, and spectral precision. These findings highlight the effectiveness of doping-based internal field modulation as a reliable and fabrication-friendly approach for advancing GaN MSM photodetector performance.

As illustrated in Fig. 3(a), PDCR values across the investigated structures demonstrate substantial improvement compared to the conventional MSM photodetectors reported in the literature. In particular, the doped MSM-PIN configuration exhibits a PDCR that exceeds 2×10^{7}, making it one of the best-performing designs when compared with recent studies such as Butun *et al.*[51] and Wen *et al.*,[52] both of which report PDCR values below 10^{6} under similar bias conditions. Likewise, the spectral responsivity distribution shown in Fig. 3(b) confirms the effectiveness of the proposed structural strategies to improve the sensitivity to UV detection while maintaining narrowband selectivity. A peak responsivity of 0.6605 A/W at 360 nm surpasses previously published values for GaN-based MSM devices without internal amplification. These results collectively underscore the success of the employed heterostructural and doping-based modifications in achieving high signal-to-noise performance and optical selectivity. Building upon these improvements, the final stage of optimization focuses on refining the geometry of the interdigitated electrode, with the goal of further improving absorption efficiency and carrier collection across the active region.

The enhanced responsivity and suppressed dark current in the MSM-PIN configuration can be physically interpreted in terms of band alignment and carrier distribution. The symmetric p- and n-type doping establishes a built-in electric field across the intrinsic GaN layer, promoting efficient electron–hole separation and suppressing recombination. Simultaneously, the AlN/GaN/InN heterointerfaces contribute polarization-induced band bending that further accelerates carrier drift toward the electrodes. These combined effects account for the significant improvements in PDCR and responsivity observed in the MSM-PIN device. This explanation is placed here, at the end of Sec. IV D, because it is in this configuration that the role of internal fields and heterointerface polarization is most critical, making it the most suitable context to interpret the observed performance gains without the need for additional figures.[11]

D. MSM-opt: sapphire/p_{GaN}/GaN/n_{GaN}/Ni/Au with electrode optimization

Following the structural and doping-based enhancements, the final optimization stage focused on refining the electrode geometry to improve optical absorption and charge collection efficiency. As detailed in Sec. III, variations in metal thickness, finger width, and spacing were evaluated to maximize the electric field uniformity across the active GaN region. The optimized design based on the MSM-PIN configuration achieved a peak photocurrent of 2.36×10^{-7} A and a dark current of 1.84×10^{-14} A, resulting in an exceptional PDCR of 2.52×10^{8} and a responsivity of 0.8159 A/W. The photoabsorption rate reached 2.25×10^{24} par/cm^3 s, indicating effective confinement of incident radiation within the mesa region. These results represent the highest responsivity and signal-to-noise performance recorded across all evaluated structures, surpassing even the doped p–i–n diode-like device described previously. Such improvements can be directly attributed to the optimized Ni/Au finger dimensions, which promote enhanced optical penetration and lateral carrier drift while minimizing electrode-induced shadowing. These findings underscore the critical role of geometrical design in complementing material and doping strategies for GaN-based MSM photodetectors. A detailed comparison of this geometry optimized device with the best-performing doped structure is presented in Fig. 4.

Figure 4 provides a comprehensive comparison between the two most advanced device architectures: the MSM-PIN structure and its geometrically optimized counterpart, MSM-Opt, which incorporates a refined electrode design for enhanced performance. As shown in Fig. 4(a), the geometry-optimized device exhibits a slightly lower photocurrent than the doped configuration at low bias but outperforms it under higher bias conditions, indicating superior field-assisted carrier transport. In Fig. 4(b), the PDCR of the geometry-optimized structure surpasses that of the doped device by more than an order of magnitude, highlighting the advantage of minimal leakage current combined with efficient photoresponse. Figure 4(c) further confirms this trend, showing a peak responsivity of 0.8159 A/W for the optimized geometry, compared to 0.6605 A/W for the doped device. These comparisons reveal that while doping strategies significantly enhance internal electric field modulation, precise control of electrode architecture can yield even greater performance gains. Therefore, electrode geometry should be considered not as a secondary adjustment but as a principal design axis in high-performance MSM photodetector development.

V. CONCLUSION

In this study, a comprehensive simulation-based optimization of GaN-based MSM photodetectors was conducted using Silvaco Atlas TCAD to enhance UV detection performance. Starting from a baseline MSM-Ref configuration, several structural and material modifications were systematically implemented and analyzed. The introduction of an MSM-Buffer heterostructure significantly improved photoabsorption and carrier separation, while the use of a SiC substrate demonstrated thermal advantages but at the cost of reduced responsivity. Further enhancements were achieved through the integration of symmetric p-type and n-type

doping around the intrinsic GaN region, forming a p–i–n diode-like structure that increased internal electric field strength and reduced recombination losses. The final optimization, involving precise adjustments to Ni/Au electrode geometry, resulted in the best overall performance, yielding a PDCR of 2.52×10^8 and a peak responsivity of 0.8159 A/W.

Figure 5 presents a consolidated overview of the key performance metrics corresponding to each MSM photodetector configuration. Figure 5(a) displays the photocurrent characteristics under forward bias conditions ranging from 0 to +3 V, demonstrating a steady improvement in current levels through successive design enhancements. Figure 5(b) illustrates the maximum photo-to-dark current ratio (PDCR) measured at +3 V, where the MSM-PIN and MSM-opt structures exhibit superior signal-to-noise performance. In Fig. 5(c), the spectral responsivity at 360 nm is compared across all configurations, with the highest value achieved in the final geometrically optimized device. Figure 5(d) shows the corresponding photoabsorption rate under +3 V, reflecting the effectiveness of

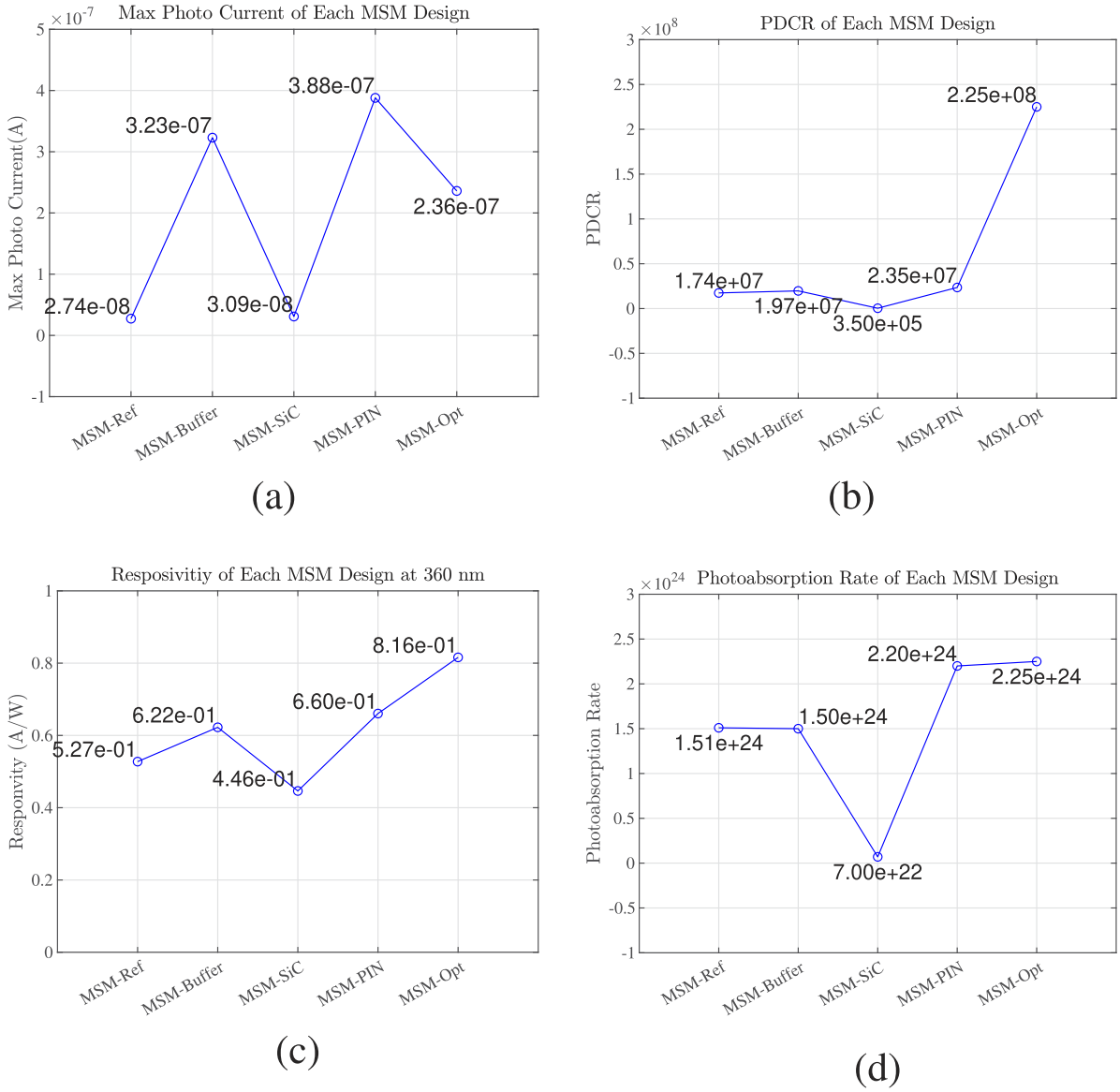

FIG. 5. Normalized performance metrics of five distinct MSM photodetector structures are presented to highlight the impact of sequential design optimizations. The graphs show (a) the maximum photocurrent under +3 V bias, (b) PDCR, (c) the spectral responsivity at 360 nm, and (d) the photoabsorption rate at +3 V. These comparative results reflect the effectiveness of structural improvements, including buffer layer engineering, substrate replacement with SiC, doping-induced internal electric field enhancement via p–i–n-like configurations, and electrode geometry refinement, each contributing incrementally to enhanced UV detection performance.

buffer layer integration and doping in enhancing photon carrier conversion. Collectively, these results highlight the critical influence of material selection, doping profile, and electrode design in advancing the efficiency and selectivity of GaN-based MSM UV photodetectors.

Comparative analyses across different architectures demonstrated that both doping and electrode design play essential roles in determining the balance between signal amplification, noise suppression, and spectral selectivity. The findings underscore that combining material-level engineering with geometrical refinement offers a powerful pathway toward the development of high-efficiency, low-noise UV photodetectors. These results provide valuable design guidelines for future fabrication efforts and suggest promising directions for the integration of GaN MSM photodetectors into high-performance optoelectronic systems. It should be noted that while the semiconductor–metal contacts were modeled using a Schottky thermionic emission framework with field-dependent mobility and, therefore, account for interface charge effects to a first order, defect-related surface states were not explicitly included in the present simulations. This idealized assumption was adopted to evaluate the intrinsic device performance, and the potential impact of non-ideal interface traps is acknowledged as a limitation requiring future experimental validation. While an explicit, spectrum-resolved mapping of native trap states or dislocation-density-coupled recombination was not undertaken here, the SRH-based effective-lifetime approach captures first-order defect effects. Accordingly, intrinsic defect density is expected to shift absolute figures of merit while preserving the observed performance ranking among the investigated architectures.

Starting from the baseline MSM-Ref structure, each subsequent design iteration was strategically introduced to address specific performance limitations: the MSM-Buffer structure incorporated a transport-enhancing buffer layer; MSM-Doped employed controlled doping profiles to modulate carrier concentration and mobility; MSM-PIN reinforced the internal electric field to promote efficient carrier separation; and finally, MSM-Optimized refined electrode geometry and material distribution for maximal extraction efficiency. Throughout this progression, nonlinear yet consistently upward trends were observed in key performance metrics such as photocurrent, PDCR, and responsivity. In particular, the enhancement in responsivity demonstrates a substantial improvement in the device's light-to-current conversion efficiency. However, this increase was not proportionally mirrored in the photoabsorption rate, indicating that the number of absorbed photons remained relatively constant while improvements in carrier separation and collection mechanisms became the dominant contributors to performance gains. These findings underscore the fact that optimizing only the optical absorption is insufficient; rather, meticulous control over carrier dynamics, via doping engineering, electric field modulation, and contact design, plays a pivotal role in achieving high-performance photodetectors. Collectively, the results confirm the necessity of a holistic design strategy and demonstrate the transformative impact of multidimensional structural optimization on the overall efficiency of GaN-based MSM photodetectors.

ACKNOWLEDGMENTS

The authors would like to express their gratitude to Adıyaman University for providing the necessary resources and facilities to conduct this research. Special acknowledgments to my colleagues for their valuable insight and technical support throughout the study. In addition, we appreciate the constructive feedback from the anonymous reviewers, which helped to improve the quality of this paper.

AUTHOR DECLARATIONS

Conflict of Interest

The authors have no conflicts to disclose.

Author Contributions

M. Kilin: Conceptualization (equal); Data curation (equal); Formal analysis (equal); Investigation (equal); Methodology (equal); Resources (equal); Software (equal); Supervision (equal); Validation (equal); Writing – original draft (equal); Writing – review & editing (equal). **O. Tanriverdi**: Formal analysis (equal); Software (equal); Writing – original draft (equal). **B. Karahan**: Formal analysis (equal); Software (equal); Writing – original draft (equal). **F. Yasar**: Conceptualization (equal); Data curation (equal); Formal analysis (equal); Investigation (equal); Project administration (equal); Resources (equal); Supervision (equal); Validation (equal); Writing – original draft (equal).

DATA AVAILABILITY

AIP Publishing believes that all datasets underlying the conclusions of the paper should be available to readers. Authors are encouraged to deposit their datasets in publicly available repositories or present them in the main paper. All research articles must include a data availability statement stating where the data can be found. In this section, authors should add the respective statement from the chart below based on the availability of data in their paper.

REFERENCES

[1] H. Morkoç, A. D. Carlo, and R. Cingolani, "Gan-based modulation doped FETs and UV detectors," Solid-State Electron. **46**, 157–202 (2002).
[2] Y. Zhang, S.-C. Shen, H. J. Kim, S. Choi, J.-H. Ryou, R. D. Dupuis, and B. Narayan, "Low-noise GaN ultraviolet p-i-n photodiodes on GaN substrates," Appl. Phys. Lett. **94**, 221109 (2009).
[3] Z. H. Zaidi and P. A. Houston, "Highly sensitive UV detection mechanism in AlGaN/GaN HEMTs," IEEE Trans. Electron Devices **60**, 2776 (2013).
[4] F. Yasar, N. Kawaguchi, T. Yanagida, I. Harrysson Rodrigues, Y. E. Ceballos, R. Prado-Rivera, and S. Keo, "Gan photonic crystals: Spectral dynamics in UV, x-ray, and alpha radiation," Adv. Photonics Res. **6**, 2400075 (2025).
[5] E. Monroy, F. Calle, C. Angulo, P. Vila, A. Sanz, J. A. Garrido *et al.*, "GaN-based solar-ultraviolet detection instrument," Appl. Opt. **37**, 5058 (1998).
[6] J. M. Van Hove, R. Hickman, J. J. Klaassen, P. P. Chow, and P. P. Ruden, "Ultraviolet-sensitive, visible-blind GaN photodiodes fabricated by molecular beam epitaxy," Appl. Phys. Lett. **70**, 2282 (1997).

[7]S. Strite and H. Morkoc, "GaN, AlN and InN: A review," J. Vac. Sci. Technol., B: Microelectron. Nanometer Struct.-Process., Meas., Phenom. **10**, 1237–1266 (1992).
[8]Q. Cai, H. You, H. Guo, J. Wang, B. Liu, Z. Xie *et al.*, "Progress on AlGaN-based solar-blind ultraviolet photodetectors and focal plane arrays," Light: Sci. Appl **10**, 94 (2021).
[9]Z. Fan, "An analysis of GaN-based ultraviolet photodetector," IOP Conf. Ser.: Mater. Sci. Eng. **738**, 012006 (2020).
[10]N. K. R. Nallabala, S. Godavarthi, V. K. Kummara, M. K. Kesarla, C. Yuvaraj, S. Kumar, N. Ravi, G. K. Guntupalli, S. A. K. Jilani, and S. V. P. Vattikuti, "High performance, self-powered and thermally stable 200–750 nm spectral responsive gallium nitride (GaN) based broadband photodetectors," Sol. Energy Mater. Sol. Cells **225**, 111033 (2021).
[11]H. Zhang, F. Liang, L. Yang, Z. Gao, K. Liang, S. Liu, Y. Ye, H. Yu, W. Chen, Y. Kang, and H. Sun, "Superior AlGaN/GaN-based phototransistors and arrays with reconfigurable triple-mode functionalities enabled by voltage-programmed two-dimensional electron gas for high-quality imaging," Adv. Mater. **36**, 2405874 (2024).
[12]M. H. Memon, H. Yu, Y. Luo, Y. Kang, W. Chen, D. Li, D. Luo, S. Xiao, C. Zuo, C. Gong, C. Shen, L. Fu, B. S. Ooi, S. Liu, and H. Sun, "A three-terminal light emitting and detecting diode," Nat. Electron. **7**, 279–287 (2024).
[13]X. Sun, D. Wang, X. Wu, J. Zhang, Y. Lin, D. Luo, F. Li, H. Zhang, W. Chen, X. Liu, Y. Kang, H. Yu, Y. Luo, B. Ge, and H. Sun, "Facile formation of van der Waals metal contact with III-nitride semiconductors," Sci. Bull. **69**, 3692–3699 (2024).
[14]M. Kilin and F. Yasar, "GaN/InN HEMT-based UV photodetector on sic with hexagonal boron nitride passivation," Photonics **12**, 950 (2025).
[15]F. Yasar, W. Fan, and Z. Ma, "Flexible amorphous GeSn MSM photodetectors," IEEE Photonics J. **10**, 2800109 (2018).
[16]Y.-L. Chu, Y.-H. Liu, T.-T. Chu, and S.-J. Young, "Improved UV-sensing of Au-decorated ZnO nanostructure MSM photodetectors," IEEE Sens. J. **22**, 5644–5650 (2022).
[17]L. Vivien, D. Marris-Morini, J.-M. Fédéli, M. Rouvière, J.-F. Damlencourt, L. E. Melhaoui *et al.*, "Metal-semiconductor-metal Ge photodetectors integrated in silicon waveguides," Appl. Phys. Lett. **92**, 151114 (2008).
[18]M. A. Alhelfi, N. M. Ahmed, M. R. Hashim, A. A. Al-Rawi, and Z. Hassan, "Simulation of optimum parameters for GaN MSM UV photodetector," AIP Conf. Proc. **1733**, 020028 (2016).
[19]S. K. Jain, S. Krishna, N. Aggarwal, R. Kumar, A. Gundimeda, S. C. Husale *et al.*, "Effect of metal contacts on a GaN/sapphire-based MSM ultraviolet photodetector," J. Electron. Mater. **47**, 6086–6090 (2018).
[20]Y. Li, Y. Liu, G. Yang, B. Bian, J. Wang, Y. Gu *et al.*, "Enhanced performance of high Al-content AlGaN MSM photodetectors by electrode modification using hexadecanethiol," Opt. Express **29**, 5466–5474 (2021).
[21]S. V. Averine, P. I. Kuznetzov, V. A. Zhitov, and N. V. Alkeev, "Solar-blind MSM photodetectors based on $Al_xGa_{1-x}N$/GaN heterostructures grown by MOCVD," Solid-State Electron **52**, 618 (2007).
[22]L. S. Chuah, Z. Hassan, and H. A. Hassan, "High-quality $In_{0.47}Ga_{0.53}N$/GaN heterostructure on Si (111) and its application to MSM detector," Microelectron. Int **25**, 3–8 (2008).
[23]C.-K. Wang, Y.-Z. Chiou, S.-J. Chang, W.-C. Lai, S.-P. Chang, C.-H. Yen, C.-C. Hung *et al.*, "GaN MSM UV photodetector with sputtered AlN nucleation layer," IEEE Sens. J. **15**, 4743–4748 (2015).
[24]N. H. Belkhir, A. Toncelli, A. K. Parchur, E. Alves, and R. Maalej, "Efficient temperature sensing using photoluminescence of Er/Yb-implanted GaN thin films," Sens. Actuators, B **248**, 769–776 (2017).
[25]A. J. Steckl, J. C. Heikenfeld, M. J. Garter, C. C. Baker, Y. Wang, D.-S. Lee, Y. Wang, and R. Jones, "Rare-earth-doped GaN: Growth, properties and fabrication of electroluminescent devices," IEEE J. Sel. Top. Quantum Electron. **8**, 749–766 (2002).
[26]M. E. Lin, B. Sverdlov, G. L. Zhou, and H. Morkoç, "A comparative study of GaN epilayers grown on sapphire and SiC substrates by plasma-assisted molecular-beam epitaxy," Appl. Phys. Lett. **62**, 3479–3481 (1993).
[27]T.-P. Chuang, N. Tumilty, C.-H. Yu, and R.-H. Horng, "Comparison of performance in GaN-HEMTs on thin SiC substrate and sapphire substrates," Chin. J. Phys. **90**, 1117 (2024).
[28]L. S. Chuah, Z. Hassan, H. A. Hassan, C. W. Chin, and S. M. Thahab, "Large-area GaN MSM photodiode using a thin low-temperature GaN cap layer," J. Nonlinear Opt. Phys. Mater **17**, 59–69 (2008).
[29]S. Fang, L. Li, D. Wang, W. Chen, Y. Kang, W. Wang *et al.*, "Breaking the responsivity-bandwidth trade-off limit in GaN photoelectrodes for high-response and fast-speed optical communication application," Adv. Funct. Mater. **33**, 2214408 (2023).
[30]W. Haiping, Y. Haifan, Y. Jiangui, Y. Minqiang, W. Lu, Z. Hong *et al.*, "Simulation study on p-GaN/AlGaN/GaN HEMT-based UV phototransistors," Micromachines Basel **10**, 213–219 (2018).
[31]S. V. Averine, Y. C. Chan, and Y. L. Lam, "Geometry optimization of interdigitated Schottky-barrier metal–semiconductor–metal photodiode structures," Solid-State Electron. **45**, 441–446 (2001).
[32]J. L. Gu, Y. F. Lu, J. Zhang, L. X. Chen, and Z. Z. Ye, "Ti/Ni/Ti/Au Ohmic contact and Schottky transformation to Al-doped ZnO thin films," J. Alloys Compd. **556**, 62–66 (2013).
[33]S. V. Averine, Y. C. Chan, and Y. L. Lam, "Optimization of high-speed MSM-photodiode structures," in *Proceedings of the COMMAD 2000: Optoelectronic and Microelectronic Materials and Devices* (IEEE, 2000), pp. 515–518.
[34]X. J. Chen, C. Y. Zhou, C. X. He, C. Wang, H. Liu, and W. Lu, "Structural and optical properties of aln/gan and AlN/AlGaN/GaN films on Si by plasma-MBE," Results Phys **12**, 1177–1181 (2018).
[35]V. Gedam, A. Pansari, A. K. Sinha, and B. K. Sahoo, "The effect of macroscopic polarization on intrinsic and extrinsic thermal conductivities of AlN," J. Phys. Chem. Solids **78**, 59–64 (2015).
[36]S. Paul, S. Hasan, and R. Islam, "Barrier height control of metal/$n^-In_{0.2}Ga_{0.8}N$ with an ultrathin interface," in *Proceedings of the 8th International Conference Electrical and Computer Engineering* (IEEE, 2014), pp. 212–215.
[37]D. Almalawi, S. Lopatin, S. Mitra, T. Flemban, A.-M. Siladie *et al.*, "Enhanced UV emission of GaN nanowires functionalized by wider band gap solution-processed p-MnO quantum dots," ACS Appl. Mater. Interfaces **12**, 34058–34064 (2020).
[38]K. Gurnett and T. Adams, "Native substrates for GaN: The plot thickens," III-Vs Rev. **19**, 39–41 (2006).
[39]X. Luo, R. Hu, S. Liu, and K. Wang, "Heat and fluid flow in high-power led packaging and applications," Prog. Energy Combust. Sci. **56**, 1–32 (2016).
[40]S. Pharkphoumy, V. Janardhanam, T.-H. Jang, K.-H. Shim, and C. J. Choi, "Correlation of crystal defects with device performance of AlGaN/GaN high-electron-mobility transistors fabricated on silicon and sapphire substrates," Electronics **12**, 1049 (2023).
[41]M. D. Vittorio, B. Poti, M. T. Todaro, M. C. Frassanito, A. Pomarico, A. Passaseo *et al.*, "High-temperature characterization of GaN-based photodetectors," Sens. Actuators, A **113**, 329–333 (2004).
[42]S. Robinson and Y. Jia, "Design of MSM photodetector: Effect of top-contact spacing on speed and transient response," Adv. Eng. Intell. Syst. **1**, 82 (2022).
[43]Y. Zhang, X. Zhang, Z. Sun, W. Wang, M. Ling, Z. Kong *et al.*, "Comparative analysis of Ni/Ag and Ni/Au contacts on GaN/AlGaN/GaN platform," Physica Status Solidi A **221**, 2400046 (2024).
[44]C. Kittel, *Introduction to Solid State Physics*, 8th ed. (John Wiley & Sons, 2005).
[45]F. Chen, X. Ji, and S. P. Lau, "Recent progress in group III-nitride nanostructures: From materials to applications," Mater. Sci. Eng.: R: Rep. **142**, 100578 (2020).
[46]J. Y. Tsao, S. Chowdhury, M. A. Hollis, D. Jena, N. M. Johnson, K. A. Jones *et al.*, "Ultrawide-bandgap semiconductors: Research opportunities and challenges," Adv. Electron. Mater. **4**, 1600501 (2018).
[47]I. Vurgaftman, J. R. Meyer, and L. R. Mohan, "Band parameters for III–IV compound semiconductors and their alloys," J. Appl. Phys. **89**, 5815–5875 (2001).
[48]S. Zarate-Galvez, A. Garcia-Barrientos, L. F. Lastras-Martinez, M. Cardenas-Juarez, S. Macias-Velasquez, L. Filipovic, and A. Arce-Casas, "Optimization of

doping concentration to obtain high internal quantum efficiency and wavelength stability in An InGaN/GaN blue light-emitting diode," ECS J. Solid State Sci. Technol. **12**, 076014 (2023).
[49]G. Cankaya and N. Ucar, "Schottky barrier height dependence on metal work function for p-type si diodes," Z. Naturforsch. A **59**, 795–798 (2004).
[50]W. Zhang, Y. X. Chen, J. Y. Yang, S. Y. Feng, B. Li, W. E. Lu *et al.*, "A novel ultraviolet photodetector with high responsivity and low operating voltage based on hybrid Si/SiC technology," IEEE Trans. Electron Devices **72**, 2411–2416 (2025).
[51]B. Butun, T. Tut, E. Ulker, T. Yelboga, and E. Ozbay, "High-performance visible-blind GaN-based p-i-n photodetectors," Appl. Phys. Lett. **92**, 033507 (2008).
[52]J. Wen, Y. Wang, B. Zhang, R. Chen, H. Zhu, X. Han, and H. Xiao, "High-performance ultraviolet photodetectors based on nanoporous GaN with a Ga_2O_3 single-crystal layer," Nanomaterials **14**, 1165 (2024).